




Microstructural analysis of titanium alloys based on high-temperature phase reconstruction

Oleksandr Lypchanskyi^{1,*} , Krzysztof Muszka¹, Bradley Wynne², Jakub Kawalko³, and Tomasz Śleboda¹

¹ Faculty of Metals Engineering and Industrial Computer Science, AGH University of Krakow, 30-059 Krakow, Poland

² Department of Mechanical and Aerospace Engineering, University of Strathclyde, Glasgow G1 1XJ, Scotland, UK

³ Academic Centre for Materials and Nanotechnology, AGH University of Krakow, 30-059 Krakow, Poland

Received: 15 April 2024

Accepted: 29 June 2024

Published online:

8 July 2024

© The Author(s), 2024

ABSTRACT

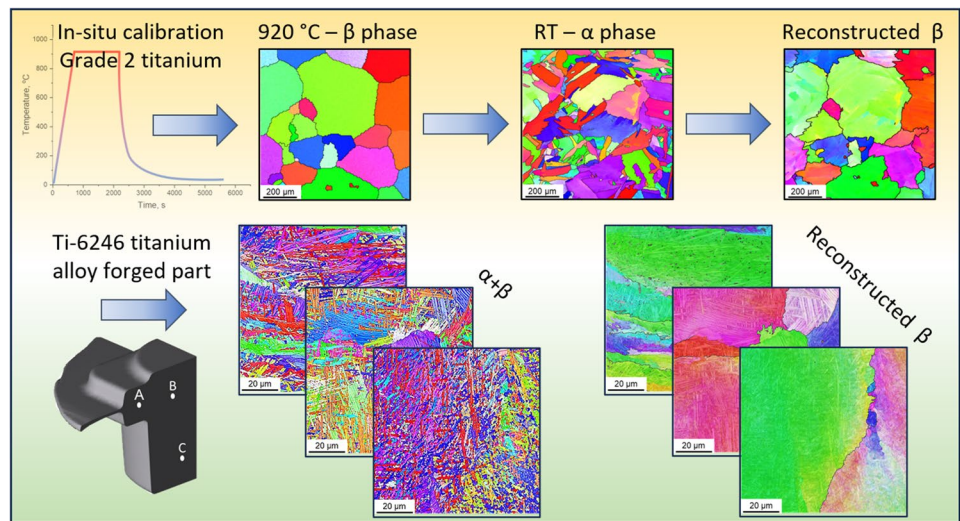
The microstructural evolution of titanium alloys under high-temperature conditions plays a key role in determining their mechanical properties and hot working behavior. This research presents an advanced method for calibrating β phase reconstruction software using in situ testing on Grade 2 titanium, which achieves accurate reconstruction of the parent β phase microstructure. In addition, unique microstructural observations in the forging of Ti-6246 titanium alloy are highlighted, demonstrating the influence of deformation parameters on the resulting β phase grain structures. Using advanced techniques such as electron backscatter diffraction and Burgers orientation relationship-based software, the research elucidates the behavior of these phases under varying thermal and deformation conditions. In Grade 2 titanium, significant grain growth and phase transformation dynamics were observed upon heating beyond the β -transus temperature during in situ calibration of β phase reconstruction software. The analysis demonstrates the effectiveness of the software in precise reconstructing the parent β phase microstructure based on the orientation of the inherited α_s phase. Furthermore, the evaluation of hot forming parameters in Ti-6246 alloy shows the influence of deformation temperature and strain rate on the resulting microstructure. Finite element method analysis coupled with dynamic material modeling elucidates the distribution of temperature, strain rate, and effective strain during forging, which aids in the qualitative assessment of hot workability. Microstructural observations in Ti-6246 alloy forging highlight the presence of elongated colonies of α_s phase precipitates, indicative of localized strain intensities and deformation temperatures. In addition, EBSD analysis coupled with β phase reconstruction reveals distinct microstructural features in different regions of the forging. In particular, regions subjected to higher strain rates exhibit elongated β phase grains with pronounced disorientation gradients, suggesting intense deformation. Conversely, optimal forging conditions lead to the appearance of unreinforced axisymmetric

Handling Editor: M. Grant Norton.

Address correspondence to E-mail: oleksandr.lypchanskyi.imf@gmail.com

β phase grains, indicating dynamic recovery processes. Pole figure analysis further emphasizes the Burgers crystallographic relationship between the α_s and β phases, confirming that deformation during forging occurs exclusively within the β phase. These results provide valuable insights into the microstructural evolution in titanium alloys under high-temperature conditions, which are essential for optimizing hot working processes and improving mechanical properties.

GRAPHICAL ABSTRACT



Introduction

Titanium and its alloys are key engineering materials in various industries, initially finding applications in the military sector and now expanding their application to various industrial domains [1, 2]. Currently, the aerospace industry represents a primary domain for titanium and its alloys, which are extensively used in the manufacture of aircraft fuselages and engine components [3, 4]. The use of these materials in compressor parts is justified by their exceptional properties, in particular high strength and corrosion resistance, which are crucial for components operating in the 500–600 °C temperature range. In addition, the suitability of these alloys for aircraft structural parts results from their excellent corrosion resistance, favorable strength-to-weight ratio, and superior machinability [5, 6]. Two-phase $\alpha + \beta$ alloys are characterized by the presence of α phase stabilizing elements such as aluminum (Al) and β phase stabilizing elements such as vanadium (V) or molybdenum (Mo). The strength of these alloys is mainly attributed to the limited solubility of β phase stabilizing elements in the α phase solid solution. However, these alloys have drawbacks such

as low thermal conductivity and relatively low susceptibility to deformation, which require careful consideration in the design of processing techniques [7].

The temperature of $\alpha + \beta \leftrightarrow \beta$ phase transformation depends on the composition of α or β phase stabilizing elements in the alloy. Elements that stabilize the β phase lower the transformation temperature, while those that stabilize the α phase increase it [8]. A variety of microstructures can be achieved in $\alpha + \beta$ alloys by carefully selecting the thermomechanical parameters of the forming process [9]. In addition, heat treatment of $\alpha + \beta$ alloys can produce finely dispersed α phase precipitates, thereby increasing the strength of the alloy [10, 11].

Ti–6Al–2Sn–4Zr–6Mo (Ti-6246) is an $\alpha + \beta$ alloy susceptible to heat treatments such as aging and solution annealing. Its microstructure is characterized by two main phases that are stable at room temperature: the α phase, which has a hexagonal close-packed (HCP) arrangement, and the β phase, which has a body-centered cubic (BCC) arrangement [12, 13]. Upon cooling from elevated temperatures, titanium alloys containing the α phase undergo various phase transformations depending on the cooling rate and the

chemical composition of the β phase. These transformations may also exhibit characteristics of martensitic transformation. In particular, the transformation of the β phase to the α_s phase proceeds consistently to completion regardless of the cooling rate [2]. Typically, α_s is the needle-like α phase that precipitates from the β phase during cooling from elevated temperatures, as opposed to the stable, globular primary alpha (α_p) present at lower temperatures. Rapid cooling rates (> 100 °C/s) in titanium alloys result in the predominant formation of needle-like α_s structure. Often the $\alpha \leftrightarrow \beta$ transformation follows the Burgers orientation relationship (BOR) [14]: $\{0001\}\alpha \parallel \{110\}\beta$; $\langle 1120 \rangle \alpha \parallel \langle 111 \rangle \beta$. The Potter, Pitsch–Schrader, and Rong–Dunlop orientation relations are alternative crystallographic models used to describe the transformations between the α and β phases in titanium alloys [15]. These relationships offer different perspectives on the orientation and misorientation angles between the phases, while the BOR model is preferred for its ability to accurately predict the most likely orientation relationships in these alloys, thereby improving the understanding of their mechanical and physical behavior [16]. According to BOR, a single β orientation can have up to 12 different α phase orientation variants, a hallmark of transformed microstructures [17]. One or more α_s phase orientations are suitable for both diffusion-driven and martensitic transformations. Despite numerous studies of phase transformations under different cooling regimes and types, the cooling process parameters that predict the transformation type remain critical [18]. Humbert et al. [19] showed that understanding the inherited crystallographic orientations of multiple α_s phase plates, strictly following BOR, facilitates the determination of the orientation of the parent β -grain. Germain et al. [20] described different variants of inherited crystallographic orientations of parent β grain and α phase, presenting a simple variant of adjacent grains in which the previous crystallographic orientation of the β grain boundary can be distinguished from the crystallographic orientation of adjacent α phase grains. Subsequently, Humbert et al. [21] used electron backscatter patterns (EBSP) to determine the average grain orientation in polycrystals. Based on the determined orientations of the α phase plates of the Ti-64 titanium alloy, they inferred a likely effect of the parent β phase state on the orientation distribution of the inherited α phase grain variants. Glavicic et al. [22] similarly analyzed the primary α_p phase and secondary α_s phase of the Ti-6246 alloy with

respect to the primary β phase using the electron backscatter diffraction (EBSD) method, demonstrating its effectiveness in identifying the ancestral orientations of β phase grains when applied to $\alpha + \beta$ alloys.

Manufacturing finished titanium alloy components requires the application of processing techniques such as hot and cold forging, drop forging, machining, joining, and occasionally extrusion. Among these techniques, forging stands out as a commonly used method for forming titanium alloy products. Dehghan-Manshadi et al. [23] investigated the microstructural evolution of Ti-6246 alloy as a function of deformation and cooling parameters. The comparative analysis revealed an increased volume fraction of the nucleated α phase in deformed microstructures, with deformation and subsequent gradual cooling leading to an expansion of the α phase volume as the cooling temperature decreased. Jackson et al. [24] conducted a study on the microstructural evolution of Ti-6246 alloy under isothermal conditions, using finite element modeling (FEM) and observing microstructures derived from the hot forging process of Ti-6246 alloy conducted below the end-of-transformation temperature. Remarkably, high strain values induced the orientation of primary α_p phase grains perpendicular to the compression axis. Alluaibi et al. [25] observed that the mechanical strength of this alloy increases as the deformation temperature approaches the β phase region up to the end-of-phase transformation temperature. In a study [26], the authors presented the results of closed die forging within the β phase range of a large aircraft engine disk made of Ti-6246 alloy, emphasizing the critical role of a low post-forging cooling rate in inducing desired microstructural changes. García et al. [27] described the industrial forging conditions of an aircraft compressor engine disk made of Ti-6246 alloy, carried out above the end-of-phase transformation temperature. Choda et al. [28] found that forging in the two-phase ($\alpha + \beta$) region has the disadvantage of reducing the fracture toughness of the resulting parts due to a structure comprising elongated α_p phase grains in the form of equiaxial lamellar segments within the β phase matrix.

Literature analysis indicates that deformation in the high-temperature β phase region of $\alpha + \beta$ titanium alloys yields products with improved mechanical properties. Understanding the behavior of this β phase at high temperatures is critical to optimizing hot working processes. However, the formation of α phase precipitates upon cooling to ambient conditions makes

Table 1 The chemical composition of the examined titanium alloys (wt.%)

Alloy	Mo	Al	Sn	Zr	Fe	O	Ti
Ti-6246	6.18	6.13	1.8	3.8	0.09	–	Bal
Grade 2	–	–	–	–	0.21	0.16	Bal

it difficult to accurately assess the evolution of the β phase microstructure at high temperatures. Therefore, the objective of this research is to validate the effectiveness of the BOR-based approach to evaluate the high-temperature β phase microstructure evolution in titanium $\alpha + \beta$ alloys. To achieve this, methods have been developed that focus on the reconstruction of the parent β grains using the α phase orientation and hence to evaluate the processing route for forging of Ti-6246 billet. Despite the availability of commercial options such as EDAX-TSL and Oxford HKL, and the free downloadable software ARPGE [29], which allow for parent phase reconstruction based on BOR, an alternative free access software [30–32] was calibrated and tested in this work.

Materials and methods

Initial material

The research used a commercially available $\alpha + \beta$ titanium alloy, designated Ti-6246, as the primary material under investigation. In addition, commercially pure α titanium, recognized as Grade 2, served as a reference material to calibrate the β phase reconstruction software. This software has been developed within [30] and now is available as a part of [31]. Table 1 presents the chemical composition of the investigated titanium alloys. Basing on dilatometric tests, it was established that the β -transus temperature in the case of the investigated Ti-6246 titanium alloy was 950 °C.

The alloys studied were provided in rod form with a diameter of approximately 50 mm. The microstructural characteristics of these alloys were then examined using scanning electron (SE) microscopy coupled with EBSD techniques. In the longitudinal section of the Ti-6246 titanium alloy rod (Fig. 1a, a1), the microstructural SE analysis revealed spheroidal dispersed grains comprising the primary α_p phase (approximately 45% by volume), accompanied by a mixture of colonies of the secondary needle-like α_s phase within a β phase matrix. The microstructure

of commercially pure Grade 2 titanium, as revealed by the EBSD–bend contrast (BC) map (Fig. 1b), exhibits equiaxial globular α phase grains with an average diameter of approximately 35 μm . Notably, both alloy microstructures demonstrate considerable homogeneity, with minimal grain elongation apparent in the rolling direction.

β phase reconstruction

Reconstruction of the high-temperature β phase was based on the β reconstruction software [30, 31]. This software serves as a critical tool for understanding and visualizing the orientation of high-temperature phases based primarily on the analysis of α phase maps derived from EBSD data. Its core functionality lies in its ability to interpret these maps, typically stored as a.ctf file, and extrapolate the orientation of the β phase based on established relationships such as the BOR. This relationship, which is fundamental to the transformation between α and β phases, is a cornerstone of the software's reconstruction process and allows for the accurate representation of phase orientations.

After importing the α phase maps, users are provided with a suite of image processing functions that facilitate grain boundary enhancement, artifact removal, and general preparation for reconstruction. Once the maps are suitably refined, the reconstruction process follows, which is characterized by a series of steps designed to identify, analyze, and reconstruct the β phase orientations corresponding to each α phase variant. Key components of the reconstruction process include the determination of potential β orientations for each α variant, the identification of correct solutions through misorientation analysis, and the iterative automation of the reconstruction process for each variant. This approach ensures accurate reconstruction of β orientations, which are critical to understanding material behavior and properties at elevated temperatures.

To reconstruct the parent β phase orientations from the α phase orientations in a Burgers transformation, there are initially six possible β orientations

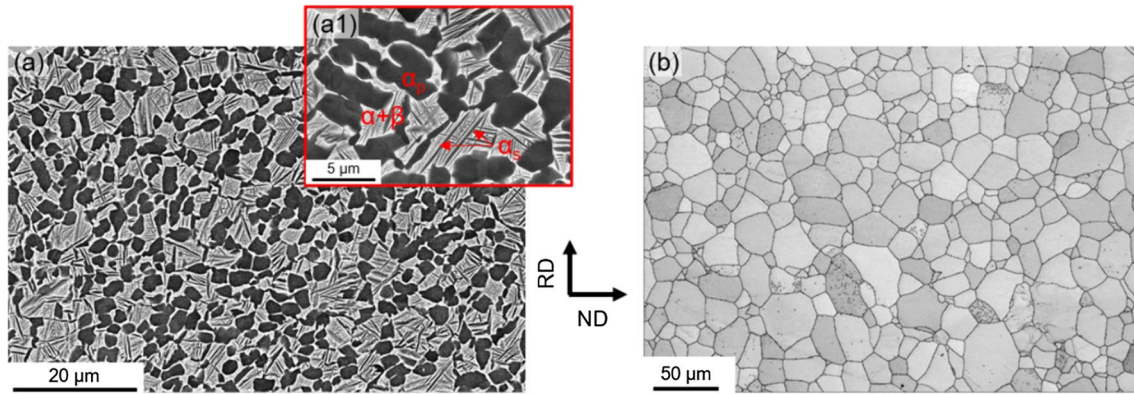


Figure 1 SE images showing the microstructure of titanium Ti-6246 alloy in the as-delivered condition (**a**, **a1**) and EBSD-BC map (**b**) showing the microstructure of commercially pure

titanium Grade 2. The microstructures are shown in longitudinal sections of the bars. RD is the rolling direction, while ND is the normal direction.

for each α orientation. The reconstruction process involves determining which of these six solutions is correct for each α orientation. This is done by analyzing the misorientations between points at the edges of a variant and adjacent points in neighboring variants. By examining these misorientations, the number of possible solutions is reduced from six to three or less, often resulting in a single unique solution. The automated reconstruction program proceeds by compiling misorientation analyses to find the most frequent solution, which is likely to be the correct one. This method successfully reconstructs the majority of α variants on the first pass. Some variants may not resolve to a single solution due to equal weighting of potential solutions. These cases are handled in a second pass using the known β orientations of neighboring variants.

The relationship between the BCC and HCP crystal structures is expressed by matrix transformations that account for 24 possible rotations, reducing the problem to identifying the correct orientation from the potential variants. Variants are identified based on a user-defined disorientation angle threshold, typically 3° , with points within this threshold marked as belonging to the same variant. The mean orientations of the variants are calculated using quaternions and crystal symmetry to avoid averaging errors. Six potential parent orientations are then determined for comparison with those derived from the inter-variant disorientation angle analyses. The most likely solution is identified by comparing the calculated disorientation angles with the potential orientations and selecting the one with the smallest

difference, assuming that this value is less than 4° . This process is repeated for all data points, with the most frequent solution selected as the correct β orientation for each variant. Unresolved cases are revisited by comparing the potential solutions to the known β orientations in neighboring variants, ensuring accurate reconstruction.

The methodology employed by the software draws heavily on established research, in particular the work of Davies [30] and Humbert et al. [32], which provides the theoretical framework for the reconstruction algorithm. By incorporating advanced techniques such as quaternion analysis and symmetry considerations, the software optimizes the accuracy and efficiency of the reconstruction process. In addition, the software integrates a cellular automata-based artifact removal tool that improves the quality of reconstructed maps by iteratively refining pixel color changes based on neighborhood analysis. This feature ensures that reconstructed maps accurately reflect the underlying material structure, free from distortions introduced by artifacts or noise in the original data. The β reconstruction software provides a comprehensive and sophisticated approach to phase reconstruction, giving researchers and engineers the tools they need to explore and understand complex material structures at high temperatures. Its meticulous methodology, based on cutting-edge research and advanced algorithms, positions it as a valuable asset in diverse industrial applications, from aerospace to materials science.

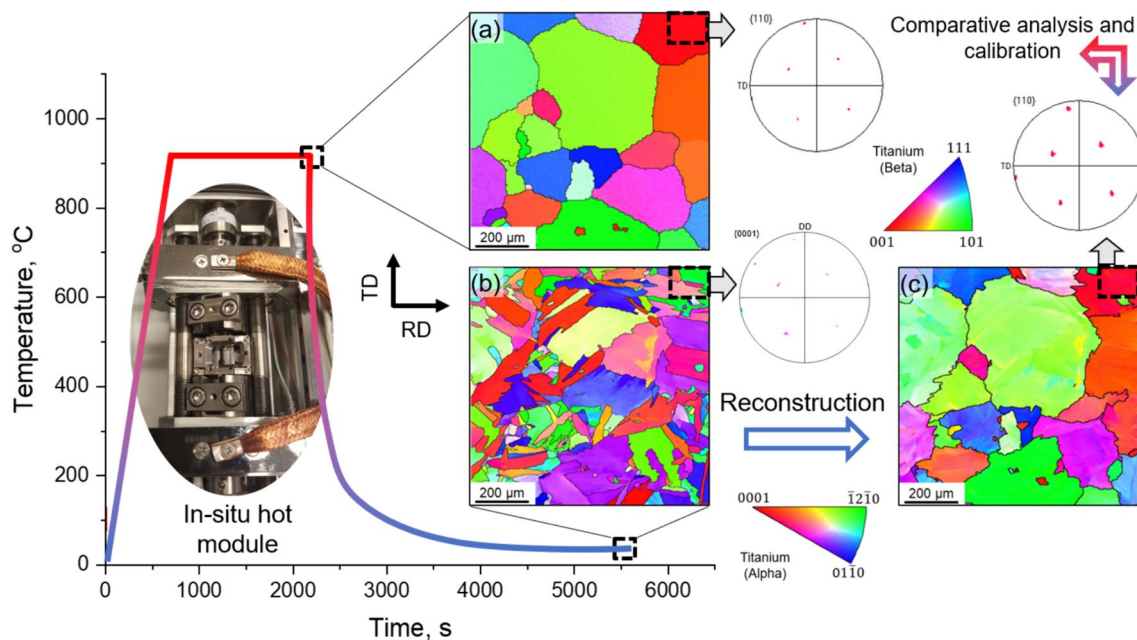


Figure 2 Illustration of the steps involved in performing software calibration for high-temperature β phase reconstruction based on in situ hot deformation tests for Grade 2 titanium. The figure shows the developed EBSD maps for key temperature con-

ditions (a, b) and the reconstructed microstructure and texture map (c) of the parent β phase grains. The texture analysis for the selected grain region is also shown.

Results

In situ calibration based on Grade 2 titanium

The calibration of the β phase reconstruction software was developed through in situ testing using the Kamrath & Weiss Tensile & Compression Module, which can handle loads up to 10 kN. This module has the capability to heat the specimen test area of SEM to the temperatures up to 1200 °C in the vacuum. The analysis was performed using commercially available Grade 2 pure titanium, which inherently maintains a complete phase in its initial state. This choice was made to streamline the calibration process and facilitate comparison of the results.

The β -transus phase transformation end point for Grade 2 is approximately 915 °C [33]. In order to achieve a fully annealed state and a homogenized microstructure of β phase grains, the α alloy under study was heated at a rate of 1.5 °C/s to the temperature of 920 °C, exceeding the phase transformation endpoint (see Fig. 2). When the stable state of the alloy is subjected to heat, a noticeable change occurs in which the fine grains of the α phase are modified by rapid atomic diffusion, ultimately resulting in grain growth. Beyond the 700 °C threshold, a recognizable

phase transformation begins. At a temperature of 920 °C, maintained for 25 min, the material undergoes a complete transformation, triggering rapid atomic diffusion and consequent β phase grain growth (Figs. 1b, 2a). The first EBSD map developed, shown in Fig. 2a, illustrates the high-temperature β phase prior to the onset of cooling. Notably, the image shows large β phase grains, with individual grains reaching a maximum circular diameter of approximately 600 μm . As the temperature decreases, the α phase undergoes a reversion process driven by the kinetics of phase transformations and diffusion phenomena. Rapid cooling is expected to result in a finer α_s phase structure by inhibiting the growth of α -grains. The kinetics of this reversion begins at the boundaries of the high-temperature β phase and progresses toward the grain center as the temperature decreases, following the BOR. In particular, Fig. 2b shows the EBSD map after cooling of the high-temperature β phase region. The observation shows that the gradual cooling results in the segregation of the α_s phase into coarse grains with irregular morphology and texture, while preserving its thermal history.

Using the acquired EBSD map of the high-temperature β phase, which delineates the parent β grains, along with the corresponding EBSD map of

the inherited α_s phase, the calibration process for the reconstruction software was performed. The inverse pole figure (IPF) maps were plotted in normal direction (ND). Figure 2c shows the resulting reconstruction of the microstructure and texture of the high-temperature β phase based on BOR. Through texture analysis within the specified grain region, a precise alignment of peaks for the $\{0001\} \alpha \parallel \{110\} \beta$ relationship is observed, confirming the retention of BOR for both the parent and inherited phases.

Evaluation of Ti-6246 titanium alloy hot forming parameters

In the following sections, the study focuses on the reconstruction and validation of the high-temperature β phase derived from the $\alpha + \beta$ titanium alloy (Ti-6246). The use of FEM analysis facilitates the determination of local hot working parameters corresponding to the target regions. In addition, local dynamic material modeling (DMM) analysis, previously described in [34], complements this effort. The synthesis of these results, along with the reconstruction of the microstructure and texture of the high-temperature β phase, aims to substantiate the efficacy of the reconstruction software and to elucidate the strain-induced changes during deformation in the β phase. In general, the hot working of Ti-6246 alloy is carried out at the temperatures above β -transus due to the low fracture toughness of the final products obtained by forging at the temperatures in the $\alpha + \beta$ range. In addition, forging in the single phase region ensures excellent mechanical properties.

Based on the DMM theory as well as numerical simulation by FEM (Fig. 3b–d), the analysis of Ti-6246 alloy forged at the temperature above β -transus under industrial conditions was carried out. The forging process consisted of heating the billet in an electric resistance furnace to the temperature of 1000 °C, followed by upset forging and final impression forging on a 1 T hammer, followed by forced air cooling. Prior to forging, the $\text{Ø}50 \times 71$ mm billet was coated with a protective silicon layer. The temperature of the tools was 250 °C, and the tools were lubricated with a graphite solution. The entire technological process was carried out at the ATI ZKM Forging Company (Stalowa Wola, Poland).

In order to evaluate the quality of the forged part obtained above the β -transus temperature, a qualitative microstructural analysis was performed using

EBSD methods. The analysis was performed on three selected areas of the forged part (Fig. 3e). These areas, marked A–C, were selected based on the results of numerical modeling of the forging process in terms of the distribution of temperature, strain rate, and effective strain values in the volume of the forged part (Fig. 3b–d). For the numerical calculations using the commercial software QForm 3D to describe the behavior of the Ti-6246 alloy, the stress–strain data obtained from plastometric tests, as well as thermal conductivity and specific heat values as a function of temperature, were used. In the industrial forging process, the initial billet temperature was 1000 °C and was then reduced by billet transport and cooling in a die cavity. A lubricant with a friction factor m of 0.1 was selected for the simulation.

According to the results of FEM analysis (Fig. 3b–d), the most extreme conditions of hot working occurred in the area A the deformation temperature reached the value of 1050 °C, the effective strain 1.8, and the strain rate about 70 s^{-1} . For area B, the temperature was 1030 °C, the effective strain 0.6, and the strain rate 40 s^{-1} . The area C of the forged part at the final stage was characterized by a forging temperature of about 1020 °C, a low strain rate (about 0.01 s^{-1}), and an effective strain of 0.4.

The 3D processing model for Ti-6246 alloy (Fig. 3f) was developed based on the methodology of DMM using the Prasad criterion of plastic flow [35]. The color scale on the presented model reflects the distribution of the η parameter (efficiency of power dissipation, which generally reflects the changes in the microstructure of the processed alloy), while the shaded areas (the negative values of the flow instability parameter ξ during deformation) indicate the possibility of the occurrence of defects related to the instability of plastic flow, such as flow localization. It should be noted that this 3D model takes into account not only the flow behavior of the investigated alloy at a constant strain value during deformation, but also gives a complete representation of the hot workability of this alloy in the investigated temperature range (800–1100 °C), true strain range (0.2–1), and strain rate range (0.01 – 100 s^{-1}). Using the 3D model, together with the information on the distribution of deformation parameters obtained earlier on the basis of FEM analysis, it is possible to evaluate the selected areas of the investigated forged part.

The analysis of the processing parameters (the distribution of temperature, strain rate, and effective

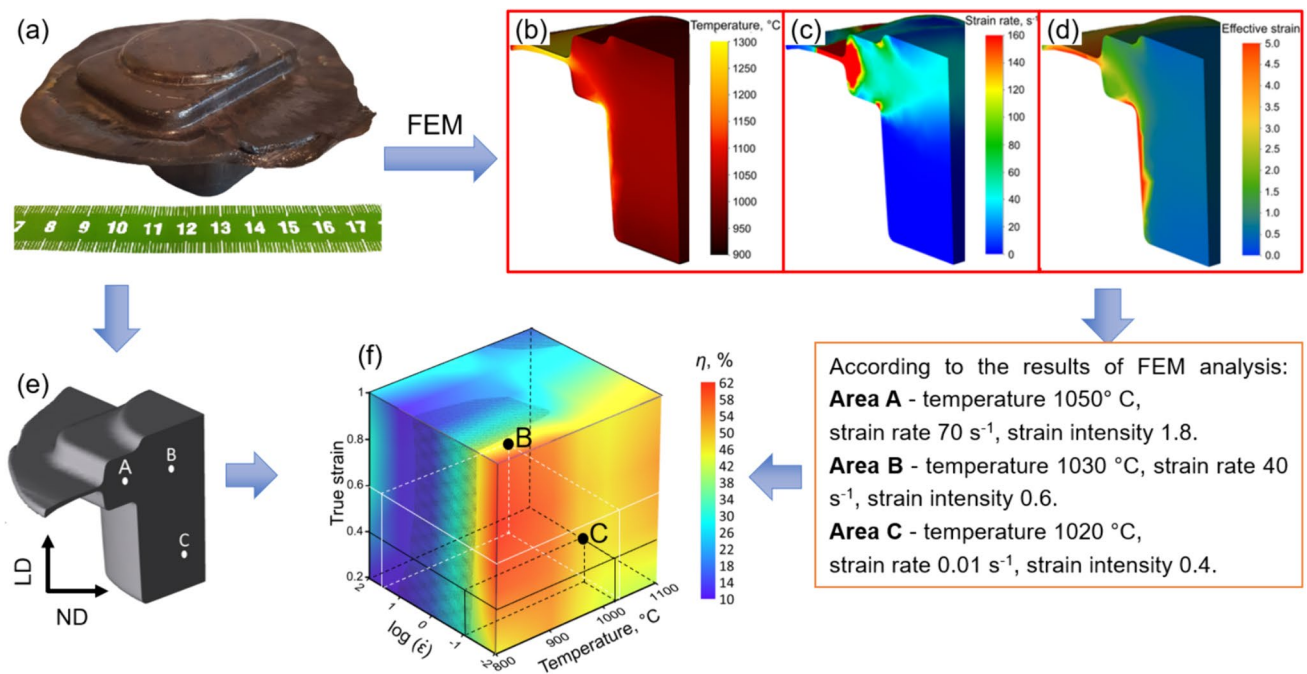


Figure 3 The forged part (a) with marked microstructural observation areas A, B, and C (e). The numerical modeling results for forging Ti-6246 alloy structural part: temperature distribution (b), strain rate distribution (c), and effective strain

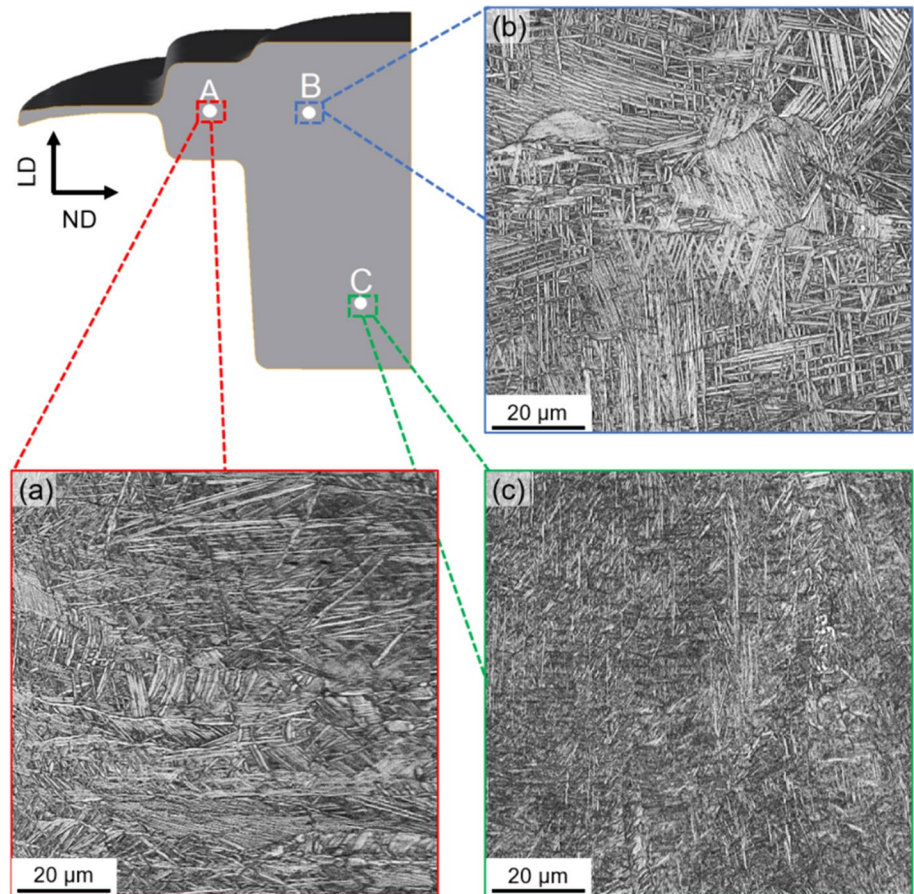
(d). The 3D processing model for Ti-6246 alloy (f). The model was developed based on previously published processing maps for Ti-6246 titanium alloy [34].

strain values) in the 3D domain of the processing model showed that the areas C ($\eta \approx 45\%$ and $\xi > 0$) and B ($\eta \approx 25\%$ and $\xi > 0$) marked on the cross section of the forged part correspond to the favorable processing parameters for hot working of the analyzed alloy. The processing parameters for area A are outside the scope of the model (the effective strain value ≈ 1). However, taking into account the nature of changes in the 3D processing model and the location of the areas of deformation stability and instability on this model, it can be assumed that the range of thermomechanical processing parameters corresponding to the point A marked on the forged part was on the border of the areas of stability and deformation instability at high strain rates ($\eta \approx 22\%$ and $\xi \approx 0$).

Figure 4 shows the microstructures observed by EBSD in selected areas (areas A–C) on the cross section of the forged part. The maps show that, in general, the forging microstructure consists of a mixture of the β phase and the colonies of the secondary needle-like α_s phase formed during cooling. Figure 4a shows the elongated colonies of α_s phase precipitates observed on the cross section of the analyzed forging in area A. This type of microstructure in area A results from higher local values of effective strain intensity and the

temperature in this area of the forged part compared to the areas B and C. High strain rates and elevated deformation temperatures facilitate rapid diffusion, promoting accelerated dislocation motion and rapid nucleation and growth of α_s phase colonies upon cooling. In addition, the visible effects related to the plastic flow instability of the alloy were not found, confirming the results of the analysis performed earlier. In the case of area B (Fig. 4b) of the forged part, there was a lower intensity of deformation as well as deformation temperature, which could cause a slower progression of nucleation and growth of α_s phase colonies in this area. In region C (Fig. 4a), there are very small precipitates of the α_s phase, which may be due to the lowest effective strain intensity and temperature found in this region based on the FEM modeling. In each case, the microstructure is considered representative of the respective regions, with the dimensions and plate size of the α_s colonies dependent on the cooling onset temperature and associated strain magnitude within the region. It can be concluded that the verification of the quality of the Ti-6246 alloy forged part in selected areas based on the 3D processing model and numerical simulation is a qualitative method for analyzing the hot workability of the investigated alloy.

Figure 4 Local microstructural observations in the form of EBSD-BC maps of a Ti-6246 alloy forging in the areas A (a), B (b), and C (c). The microstructures represent the distribution of α_s colonies in the β phase grains as a function of the strain parameters corresponding to these areas.



Reconstruction of the high-temperature β phase of the Ti-6246 titanium alloy

EBSD analysis can be used to reconstruct the microstructure of the forged part, which is predominantly composed of the α_s colonies. This reconstruction is based on the Burgers relationship, which elucidates the crystallographic orientations between the inherited α_s phase and the parent high-temperature β phase. Crystallographic orientation maps of the α_s phase within the β phase matrix for the regions examined A-C are shown in Fig. 5. The IPF maps were plotted in the Z direction corresponding to the transverse direction (TD) in the loading direction (LD) normal direction (ND) plane. These maps allow a direct examination of the microstructural evolution during deformation in relation to the β phase. The basic principles and the reconstruction software used are described in the previous sections. Histograms illustrating the distribution of α_s phase grain boundaries (Fig. 5a1, b1, c1), derived from the EBSD-IPF maps for the respective regions of the examined forging cross

section, show prominent frequency peaks corresponding to misorientation angles of 10° , 30° , 60° and 90° in all histograms.

The crystallographic orientation maps of the high-temperature β phase were reconstructed using the crystallographic orientation maps of the α_s phase obtained by the EBSD method in software based on the BOR as described in [30]. The resulting IPF maps of the reconstructed β phase, derived from the EBSD maps of the α_s phase over different regions, are shown in Fig. 6. These reconstructed maps delineate the grains of the β phase against the background of the lamellar α_s phase. Notably, the case maps highlight only high-angle boundaries $> 15^\circ$ of the β phase grains, represented by black lines.

The β phase grains within region A exhibited the highest strain values as shown in Fig. 6a. The increased strain rate intensity observed in this region may have hindered the progress of recrystallization. Notably, despite the significant elongation of β phase grains along the flow direction due to the high strain value, they maintained their structural integrity and

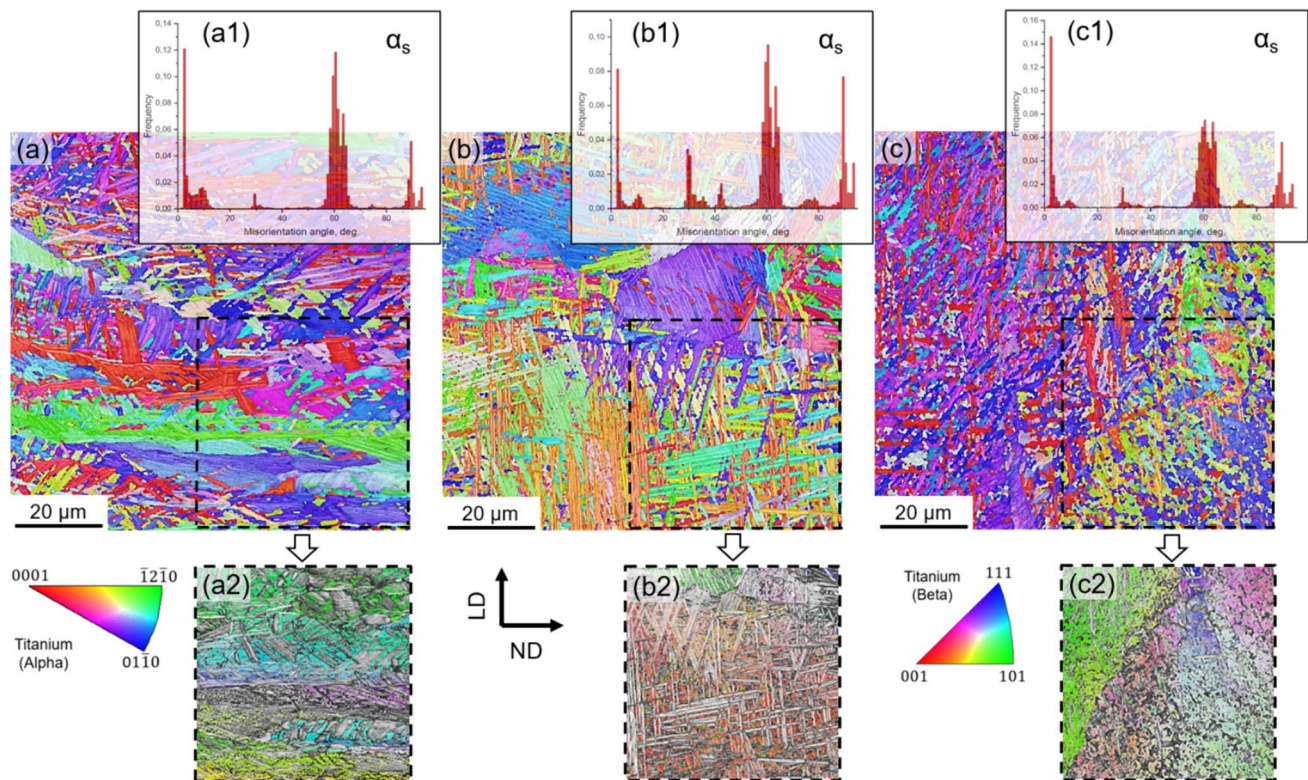


Figure 5 EBSD-IPF maps of the distribution of α_s colonies in the matrix of the β phase for the areas A (**a**), B (**b**), and C (**c**) observed on the cross section of the Ti-6246 alloy forging. EBSD analyses in the form of histograms of grain boundary distribu-

tions of the α_s phase (**a1**, **b1**, **c1**) are also presented. The combined band contrast (BC) map with a superimposed IPF map for the β phase from the IPF map areas is shown in Figures **a2**, **b2**, **c2**. LD is the loading direction, while ND is the normal direction.

exhibited cohesion without fragmentation. In addition, these grains exhibited significant local gradients in disorientation, indicating a strongly deformed microstructure.

In region B (Fig. 5b), the α_s phase exhibits an optimal structure, which is a direct result of the development of the β phase microstructure and the application of an optimal cooling rate. The local deformation conditions, which include temperature, strain rate, and strain value during forging, have created a favorable environment for dynamic recovery processes. As a result, a non-reinforced axisymmetric β phase grain morphology has emerged. At the same time, the dynamic recovery process under these conditions has precluded recrystallization due to insufficient momentum for nucleation.

In Fig. 6a, a slowdown in the formation of recrystallization nuclei within the β phase was observed in region A, correlating with the minimum strain rate and intensity there. This observation finds its rationale in the small strain intensity and the associated

dynamic recovery process that occurs under these circumstances. Singular nuclei manifest exclusively, resulting from the collapse of curvature along the β grain boundaries, particularly where the steepest gradient of crystallographic orientations within the β grain prevails. Thus, it can be concluded that only the nascent stage of β phase recrystallization is evident in the region under investigation, which is particularly constrained by the conspicuous presence of large grains.

For a more in-depth analysis, distinct subregions were selected within each examined area across the forging cross section (A1, B1, C1). Pole figures were then constructed for both the α_s phase and the reconstructed β parent phase (Fig. 6 a1, a2, b1, b2, c1, c2). Examination of the presented pole figures reveals a conspicuous adherence to the Burgers relation between the inherited phase (α_s) and the parent phase (β), with all poles of the {0001} and {110} planes perfectly coinciding. This phenomenon clearly demonstrates that within the subregions studied, α_s phase

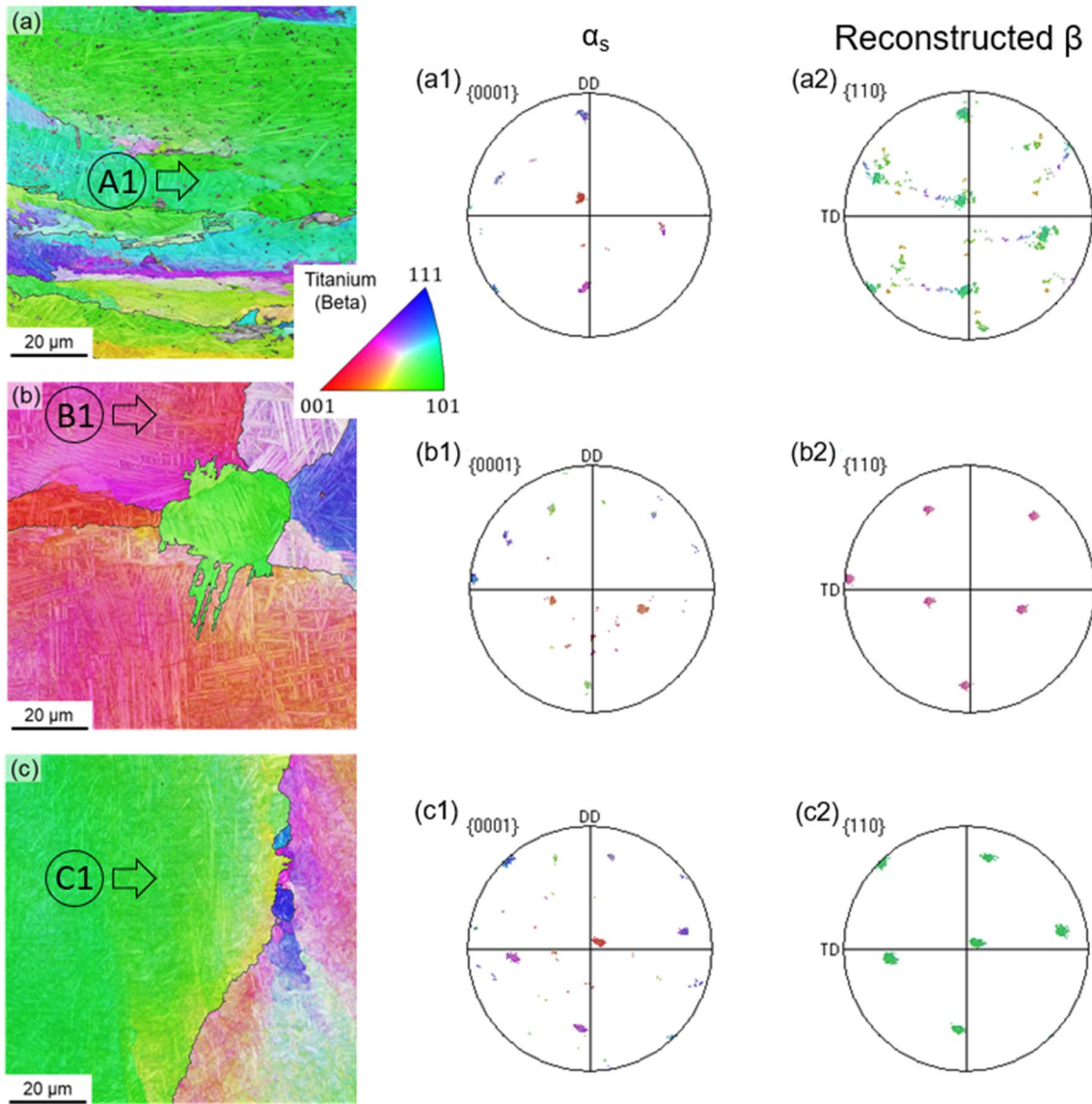


Figure 6 IPF maps after high-temperature β phase reconstruction for the areas A (a), B (b), and C (c). Comparative analysis of pole figures of α_s phase (a1, b1, c1) and reconstructed β phase

(a2, b2, c2) from selected areas A1, B1, C1 grains. The analysis developed to confirm BOR $\{0001\}\alpha \parallel \{110\}\beta$.

grains originate from a single β phase grain. Furthermore, the persistence of the Burgers crystallographic relationship in all cases studied supports the occurrence of deformation exclusively within the β phase during forging, which occurs at the temperature where only the β phase is present and susceptible to deformation. Conversely, in regions of the forging exposed to temperatures below the termination point of the phase transformation, where deformation would include the α phase, the Burgers crystallographic relationship would not apply.

Discussion

The analysis of Grade 2 titanium during in situ testing provides a benchmark for understanding the response of α phases under extreme thermal conditions. The microstructural changes observed, particularly the transformation of fine α phase grains upon heating (Fig. 2), highlight the susceptibility of the alloy to rapid atomic diffusion [36] and subsequent grain growth of β phase grains (Figs. 1b, 2a). This phenomenon, which culminates in the formation of large α

grains after cooling, underscores the intricate interplay between temperature, phase transformation kinetics, and microstructural evolution. The cooling process reduces the mobility of dislocations, although they remain as mobile entities capable of interacting with grain boundaries [37]. In addition, the study of Grade 2 titanium serves as a basis for calibrating β phase reconstruction software, which is essential for accurate interpretation of microstructural data in more complex alloy systems. By leveraging the unique characteristics of Grade 2 titanium, such as its homogeneous microstructure [38] and known phase transformation endpoints, researchers can validate and refine software algorithms, increasing their application in the analysis of more complex alloy systems.

The BOR remains a cornerstone of the analysis, facilitating the accurate reconstruction of β phase orientations from α phase maps derived from EBSD data. An assessment of the forged alloy's quality within the single phase region (β phase) was conducted by employing EBSD analysis across three distinct regions (Fig. 4). The absence of detectable manifestations of plastic flow instability (Fig. 5), sometimes observed in other titanium alloys [39–41], confirmed previous analyses (see Fig. 4). The investigation revealed that the deformation during forging occurred within the temperature regime where only the β phase was dominant and thus underwent only plastic deformation (Fig. 6). The behavior of the high-temperature β phase highlights the remarkable ability of the alloy to withstand severe deformation conditions while maintaining structural integrity. In particular, the β phase exhibits elongation along the flow direction, indicating significant plastic deformation (Fig. 6a). This resistance to fragmentation underscores the robust mechanical properties of the alloy, which are critical for applications requiring high strength and durability [42].

A key finding is the inhibition of recrystallization [43] within regions of intense deformation, which is attributed to elevated strain values (Fig. 6a). The phenomenon of high strain rates is known for its propensity to induce dislocation stacking and accelerate phase transformation due to the substantial accumulation of deformation storage energy [44]. Conversely, regions experiencing optimal deformation conditions facilitate dynamic recovery processes [45], promoting the emergence of an unreinforced axisymmetric β phase grain morphology.

Central to the analysis is the Burgers relationship, which remains strikingly evident in all regions

examined. This crystallographic orientation between the α_s and β phases explains the exclusive deformation that occurs within the β phase during forging, testifying to the alloy's unique response to thermal and mechanical parameters [46]. By elucidating the intricate mechanisms that drive microstructural evolution, this study lays the groundwork for improved alloy design and process optimization, with far-reaching implications for industries that rely on high-performance materials, such as aerospace [47], medicine, and automotive.

Conclusion

The studies of the high-temperature reconstruction of the parent β phase for Grade 2 titanium and titanium alloy Ti-6246 provide conclusive findings. The following key conclusions can be drawn as follows:

1. The in situ calibration process performed on Grade 2 titanium provided concrete evidence of the software's effectiveness, demonstrating its ability to accurately reconstruct the high-temperature β phase microstructure in Ti-6246 alloy.
2. Examination of Grade 2 titanium's phase transformation dynamics revealed significant grain growth within the β phase upon surpassing the β -transus temperature. This observation highlights the material's sensitivity to the temperature variations and underscores the importance of precise temperature control in industrial forging processes to achieve desired microstructural properties and mechanical performance.
3. Detailed analysis of the EBSD maps revealed distinct microstructural features, in particular the presence of elongated colonies of secondary α_s phase precipitates. These observations were particularly pronounced in regions subjected to elevated local effective strain and temperature intensities, indicating facilitated dislocation motion and accelerated nucleation kinetics.
4. The observed adherence to the Burgers relationship across different forging regions underscores the predominant influence of β phase deformation during hot working. These results show the critical role of precise temperature and strain intensity control in controlling the microstructural evolution of the Ti-6246 alloy, providing invaluable insights

for optimizing industrial hot forging processes and ensuring superior product quality.

Acknowledgements

Financial support from the National Science Center of Poland Project No. UMO-2015/19/B/ST8/01079 is acknowledged.

Author contributions

Oleksandr Lypchanskyi contributed to investigation, methodology, validation, writing—original draft, and writing—review and editing. Krzysztof Muszka was involved in conceptualization, investigation, funding acquisition, validation, and project administration and provided software. Bradley Wynne provided software and contributed to data analysis. Jakub Kawalko was involved in investigation and validation. Tomasz Śleboda contributed to supervision, formal analysis, and writing—review and editing.

Data availability

Data will be made available upon request.

Declarations

Conflict of interest The authors declare that they have no conflict of interest.

Open Access This article is licensed under a Creative Commons Attribution 4.0 International License, which permits use, sharing, adaptation, distribution and reproduction in any medium or format, as long as you give appropriate credit to the original author(s) and the source, provide a link to the Creative Commons licence, and indicate if changes were made. The images or other third party material in this article are included in the article's Creative Commons licence, unless indicated otherwise in a credit line to the material. If material is not included in the article's Creative Commons licence and your intended use is not permitted by statutory regulation or exceeds the

permitted use, you will need to obtain permission directly from the copyright holder. To view a copy of this licence, visit <http://creativecommons.org/licenses/by/4.0/>.

References

- [1] Leyens C, Peters M (2003) Titanium and titanium alloys: fundamentals and applications. WILEY-VCH, Weinheim. <https://doi.org/10.1002/3527602119>
- [2] Boyer R, Welsch G, Collings EW (1998) Materials properties handbook: titanium alloys. ASM International, OH
- [3] Huda Z, Edi P (2013) Materials selection in design of structures and engines of supersonic aircrafts: a review. Mater Des 46:552–560. <https://doi.org/10.1016/j.matdes.2012.10.001>
- [4] Williams JC, Starke EA (2003) Progress in structural materials for aerospace systems. Acta Mater 51(19):5775–5799. <https://doi.org/10.1016/j.actamat.2003.08.023>
- [5] Donachie MJ (2000) Titanium: a technical guide, 2nd ed, ASM International
- [6] Jaffery SI, Mativenga PT (2009) Assessment of the machinability of Ti–6Al–4V alloy using the wear map approach. Int J Adv Manuf Technol 40(7–8):687–696. <https://doi.org/10.1007/s00170-008-1393-9>
- [7] Lütjering G, Williams JC (2007) Titanium: engineering materials and processes. Springer, Berlin. <https://doi.org/10.1007/978-3-540-73036-1>
- [8] Huang S, Zhao Q, Wu C et al (2021) Effects of β -stabilizer elements on microstructure formation and mechanical properties of titanium alloys. J Alloys Compd 876:160085. <https://doi.org/10.1016/j.jallcom.2021.160085>
- [9] Kuhlman GW, Kim Y-W, Boyer RR (1991) A critical appraisal of thermomechanical processing of structural titanium alloys. In: Microstructure/property relationships in titanium aluminides and alloys. Warrendale, TMS, USA
- [10] Welk BA, Taylor N, Kloenne Z et al (2021) Use of alloying to effect an equiaxed microstructure in additive manufacturing and subsequent heat treatment of high-strength Titanium Alloys. Metall Mater Trans A 52:5367–5380. <https://doi.org/10.1007/s11661-021-06475-3>
- [11] Du Z, Xiao S, Xu L et al (2014) Effect of heat treatment on microstructure and mechanical properties of a new β high strength titanium alloy. Mater Des 55:183–190. <https://doi.org/10.1016/j.matdes.2013.09.070>
- [12] Lu L, Zhang Y, Song K et al (2021) Structural characterization and nanoscale strain field analysis of α/β interface

- layer of a near α titanium alloy. *Nanotechnol Rev* 10:1197–1207. <https://doi.org/10.1515/ntrev-2021-0085>
- [13] Krawczyk J, Łukaszek-Solek A, Dąbrowski R (2015) The role of the deformation conditions in the evolution of the microstructure of Ti–6Al–2Sn–4Zr–6Mo alloy. *Key Eng Mater* 641:116–119. <https://doi.org/10.4028/www.scientific.net/KEM.641.116>
- [14] Burgers WG (1934) On the process of transition of the cubic body centered modification into the hexagonal close packed modification of zirconium. *Physica* 1:561–586. [https://doi.org/10.1016/S0031-8914\(34\)80244-3](https://doi.org/10.1016/S0031-8914(34)80244-3)
- [15] Zhang M-X, Kelly PM (2005) Edge-to-edge matching and its applications: part I application to the simple HCP/BCC system. *Acta Mater* 53:1073–1084. <https://doi.org/10.1016/j.actamat.2004.11.007>
- [16] Tong V, Joseph S, Ackerman AK et al (2017) Using transmission Kikuchi diffraction to characterise α variants in an $\alpha+\beta$ titanium alloy. *J Microsc* 267(3):318–329. <https://doi.org/10.1111/jmi.12569>
- [17] Gey N, Humbert M (2002) Characterization of the variant selection occurring during the $\alpha\rightarrow\beta\rightarrow\alpha$ phase transformations of a cold rolled titanium sheet. *Acta Mater* 50:277–287. [https://doi.org/10.1016/S1359-6454\(01\)00351-2](https://doi.org/10.1016/S1359-6454(01)00351-2)
- [18] Baeslack WA, Mullins FD (1982) Phase transformation in a welded near-alpha titanium alloy—IMI 829. *J Mater Sci Lett* 1:371–373. <https://doi.org/10.1007/BF00724841>
- [19] Humbert M, Wagner F, Moustahfid H et al (1995) Determination of the orientation of a parent β grain from the orientations of the inherited α plates in the phase transformation from body-centred cubic to hexagonal close packed. *J Appl Cryst* 28:571–576. <https://doi.org/10.1107/S0021889895004067>
- [20] Germain L, Gey N, Humbert M (2007) Reliability of reconstructed β -orientation maps in titanium alloys. *Ultramicrosc* 107:1129–1135. <https://doi.org/10.1016/j.ultramic.2007.01.012>
- [21] Humbert M, Gey N, Muller J et al (1996) Determination of a mean orientation from a cloud of orientations. Application to electron back-scattering pattern measurements. *J Appl Cryst* 29:662–666. <https://doi.org/10.1107/S0021889896006693>
- [22] Glavicic MG, Bartha BB, Jha SK et al (2009) The origins of microtexture in duplex Ti alloys. *Mater Sci Eng A* 513–514:325–328. <https://doi.org/10.1016/j.msea.2009.02.003>
- [23] Dehghan-Manshadi A, Dippenaar RJ (2012) Strain-induced phase transformation during thermo-mechanical processing of titanium alloys. *Mater Sci Eng A* 552:451–456. <https://doi.org/10.1016/j.msea.2012.05.069>
- [24] Jackson M, Dashwood RJ, Christodoulou L et al (2002) Isothermal subtransus forging of Ti 6Al–2Sn–4Zr–6Mo. *J Light Met* 2:185–195. [https://doi.org/10.1016/S1471-5317\(02\)00044-5](https://doi.org/10.1016/S1471-5317(02)00044-5)
- [25] Alluaibi MH, Rusea A, Cojocaru VD (2018) Influence of thermomechanical processing at temperatures above β -transus on the microstructural and mechanical characteristics of the Ti-6246 alloy. *UPB Sci Bull Ser B* 80(1):245–258
- [26] Uginet JF, Albert V (2007) Close die forging of Ti 6246 engine disks. Aubert and Duval Pamiers France, 11th WC Titanium, Kyoto
- [27] García AMM (2011) BLISK fabrication by linear friction welding. *Adv Gas Turbine Tech* 18:411–435. <https://doi.org/10.5772/21278>
- [28] Choda T, Oyama H, Murakami S (2015) Technologies for process design of titanium alloy forging for aircraft parts. *Kobelco Tech Rev* 33:44–49
- [29] Cayron C (2007) ARPGE: a computer program to automatically reconstruct the parent grains from electron backscatter diffraction data. *J Appl Cryst* 40:1183–1188. <https://doi.org/10.1107/S0021889807048777>
- [30] Davies PS (2009) An investigation of microstructure and texture evolution in the Near- α Titanium Alloy Timetal @ 834. Ph.D. thesis, Department of Engineering Materials, The University of Sheffield
- [31] Silva BF, Jackson M, Fox K et al (2023) Tool for automatic macrozone characterization from EBSD data sets of titanium alloys. *J Appl Crystallogr* 56:737–749. <https://doi.org/10.1107/S1600576723003862>
- [32] Gey N, Humbert M (2002) Characterization of variant selection occurring during the $\alpha\rightarrow\beta\rightarrow\alpha$ phase transformations of a cold rolled titanium sheet. *Acta Mater* 50:277–287. [https://doi.org/10.1016/S1359-6454\(01\)00351-2](https://doi.org/10.1016/S1359-6454(01)00351-2)
- [33] Singh G, Souza PM (2023) Hot deformation behavior of a novel alpha+beta titanium alloy TIMETAL@407. *J Alloys Compd* 935:167970. <https://doi.org/10.1016/j.jallcom.2022.167970>
- [34] Lypchanskyi O, Śleboda T, Wojtaszek M et al (2021) The analysis of flow behavior of Ti–6Al–2Sn–4Zr–6Mo alloy based on the processing maps. *Int J Mater Form* 14:523–532. <https://doi.org/10.1007/s12289-019-01533-z>
- [35] Prasad YVRK, Seshacharyulu T (1998) Processing maps for hot working of titanium alloys. *Mater Sci Eng A* 243(1–2):82–88. [https://doi.org/10.1016/S0921-5093\(97\)00782-X](https://doi.org/10.1016/S0921-5093(97)00782-X)
- [36] Lin YC, Huang J, He D-G et al (2019) Phase transformation and dynamic recrystallization behaviors in a Ti55511 titanium alloy during hot compression. *J Alloys Compd*

- 795:471–482. <https://doi.org/10.1016/j.jallcom.2019.04.319>
- [37] Zhang J-Y, Sun Z-P, Qiu D (2023) Dislocation-mediated migration of the α/β interfaces in titanium. *Acta Mater* 261:119364. <https://doi.org/10.1016/j.actamat.2023.119364>
- [38] Qarni MJ, Sivaswamy G, Rosochowski A et al (2017) On the evolution of microstructure and texture in commercial purity titanium during multiple passes of incremental equal channel angular pressing (I-ECAP). *Mater Sci Eng A* 699:31–47. <https://doi.org/10.1016/j.msea.2017.05.040>
- [39] Lypchanskyi O, Śleboda T, Łukaszek-Solek A et al (2021) Application of the strain compensation model and processing maps for description of hot deformation behavior of metastable β titanium alloy. *Materials* 14(8):2021. <https://doi.org/10.3390/ma14082021>
- [40] Zyguła K, Lypchanskyi O, Łukaszek-Solek A et al (2024) A comprehensive study on hot deformation behavior of the metastable β titanium alloy prepared by blended elemental powder metallurgy approach. *Metall Mater Trans A* 55:933–954. <https://doi.org/10.1007/s11661-024-07297-9>
- [41] Jiang Y-Q, Lin YC, Wang G-Q et al (2021) Microstructure evolution and a unified constitutive model for a Ti-55511 alloy deformed in β region. *J Alloys Compd* 870:159534. <https://doi.org/10.1016/j.jallcom.2021.159534>
- [42] Gatina SA, Polyakova VV, Polyakov AV et al (2022) Microstructure and mechanical properties of β -titanium Ti-15mo alloy produced by combined processing including ECAP-conform and drawing. *Mater* 15(23):8666. <https://doi.org/10.3390/ma15238666>
- [43] Alaneme KK, Okotete EA (2019) Recrystallization mechanisms and microstructure development in emerging metallic materials: a review. *J Sci Adv Mater Devices* 4(1):19–33. <https://doi.org/10.1016/j.jsamd.2018.12.007>
- [44] Souza PM, Beladi H, Singh RP et al (2018) An analysis on the constitutive models for forging of Ti6Al4V alloy considering the softening behavior. *J Mater Eng Perform* 27:3545–3558. <https://doi.org/10.1007/s11665-018-3402-y>
- [45] Zyguła K, Wojtaszek M, Śleboda T et al (2021) The influence of induction sintering on microstructure and deformation behavior of Ti–5Al–5Mo–5V–3Cr Alloy. *Metall Mater Trans A* 52:1699–1713. <https://doi.org/10.1007/s11661-021-06179-8>
- [46] Muszka K, Lopez-Pedrosa M, Raszka K et al (2014) The impact of strain reversal on microstructure evolution and orientation relationships in Ti–6Al–4V with an initial alpha colony microstructure. *Metall Mater Trans A* 45:5997–6007. <https://doi.org/10.1007/s11661-014-2590-9>
- [47] Muszka K, Madej L, Wynne BP (2016) Application of the digital material representation to strain localization prediction in the two phase titanium alloys for aerospace applications. *Arch Civ Mech Eng* 16(2):224–234. <https://doi.org/10.1016/j.acme.2015.10.003>

Publisher's Note Springer Nature remains neutral with regard to jurisdictional claims in published maps and institutional affiliations.